Human proteinase 3 resistance to inhibition extends to alpha-2 macroglobulin

Koffi N'Guessan, Renata Grzywa, Seda Seren, Guillaume Gabant, Maria Juliano, Marc Moniatte, Alain van Dorssaeler, Joseph Bieth, Christine Kellenberger, Francis Gauthier, et al.

ARTICLE

Human proteinase 3 *resistance* to inhibition extends to alpha-2 macroglobulin

Koffi N'Guessan[1,2], Renata Grzywa[3§], Seda Seren[1,2§], Guillaume Gabant[4], Maria A. Juliano[5], Marc Moniatte[6], Alain van Dorsselaer[7], Joseph Bieth[8], Christine Kellenberger[9], Francis Gauthier[1,2], Magdalena Wysocka[10], Adam Lesner[10], Marcin Sienczyk[3], Martine Cadene[4] and Brice Korkmaz[1,2]*

[1]INSERM UMR-1100, CEPR « Centre d'Etude des Pathologies Respiratoires », 37032, Tours, France
[2]Université de Tours, 37032, Tours, France
[3]Wroclaw University of Science and Technology, Faculty of Chemistry, Division of Medicinal, Chemistry and Microbiology, Wyb. Wyspianskiego 27, 50-370 Wroclaw, Poland
[4]Centre de Biophysique Moléculaire, UPR4301 CNRS, 45071 Orléans, France
[5]Universidade Federal de São Paulo, Escola Paulista Medicina, Departamento de Biofísica, São Paulo, SP, Brazil
[6]Proteomics Core Facility, École Polytechnique Fédérale de Lausanne (EPFL), CH-1015 Lausanne, Switzerland
[7]LSMBO, Institut Pluridisciplinaire Hubert Curien, CNRS UMR-7178 (CNRS-UdS), ECPM, 67087 Strasbourg, France
[8]Laboratoire d'Enzymologie, INSERM UMR-392, Université Louis Pasteur de Strasbourg, 67400 Illkirch, France
[9]Laboratoire de Chimie Bactérienne CNRS UMR-7283, 13402, Marseille, France
[10]University of Gdansk, Faculty of Chemistry, 80-309 Gdansk, Poland
[§]Equal contribution

***Corresponding author:** Brice Korkmaz

INSERM UMR-1100 "Centre d'Etude des Pathologies Respiratoires (CEPR)",
Université de Tours, Faculté de Médecine
10 Bld. Tonnellé, 37032, Tours, France
e-mail: brice.korkmaz@inserm.fr
Tel: 0033 2 47 36 63 86
https://cepr.inserm.univ-tours.fr/

Running title: α2-macroglobulin and proteinase 3

Keywords: α2-macroglobulin, proteinase 3, proteolysis, serine proteinase

Abbreviations: α1-PI, alpha-1-proteinase inhibitor; α2-M, α2-macroglobulin, ABZ, *ortho*-aminobenzoic acid; AMC, aminomethyl coumarin; COPD, chronic obstructive pulmonary disease, h, human; HPLC, high performance liquid chromatography; CatG; cathepsin G, EDDnp, *N*-(2.4-dinitrophenyl)ethylenediamine; FRET, fluorescence resonance energy transfer; GPA, granulomatosis with polyangiitis; MS, mass spectrometry; NE, neutrophil elastase; NSP, neutrophil serine proteinase; PBS, phosphate-buffered saline; PR3, proteinase 3.

Abstract

Neutrophils contain at least four serine endopeptidases namely elastase (NE), proteinase 3 (PR3), cathepsin G (CatG) and NSP4, which contribute to the regulation of infection and of inflammatory processes. In physiological conditions, endogenous inhibitors including α2-macroglobulin (α2-M), serpins (α1-proteinase inhibitor (α1-PI)), monocyte neutrophil elastase inhibitor (MNEI), α1-antichymotrypsin) and locally produced chelonianins (elafin, SLPI) control excessive proteolytic activity of neutrophilic serine proteinases. In contrast to human elastase (hNE), hPR3 is weakly inhibited by α1-PI and MNEI but not by SLPI. α2-M is a large spectrum inhibitor that traps a variety of proteinases in response to cleavage(s) in its bait region. We report here that α2-M was more rapidly processed by hNE than hPR3 or hCatG. This was confirmed by the observation that the association between α2-M and hPR3 is governed by a k_{ass} in the $\leq 10^5$ $M^{-1}.s^{-1}$ range. Since α2-M-trapped proteinases retain peptidase activity, we first predicted the putative cleavage sites within the α2-M bait region (residues 690-728) using kinetic and molecular modeling approaches. We then identified by mass spectrum analysis the cleavage sites of hPR3 in a synthetic peptide spanning the 39-residue bait region of α2-M (39pep-α2-M). Since the 39pep-α2-M peptide and the corresponding bait area in the whole protein do not contain sequences with a high probability of specific cleavage by hPR3 and were indeed only slowly cleaved by hPR3, it can be concluded that α2-M is a poor inhibitor of hPR3. The resistance of hPR3 to inhibition by endogenous inhibitors explains at least in part its role in tissue injury during chronic inflammatory diseases and its well-recognized function of major target auto-antigen in granulomatosis with polyangiitis.

INTRODUCTION

Polymorphonuclear neutrophils, the most abundant blood cells of innate immunity, constitute the first line of defense against pathogens in inflammatory conditions. Their cytoplasmic granules store four active forms of neutrophil serine proteinases (NSPs), neutrophil elastase (NE), proteinase 3 (PR3), cathepsin G (GC) and neutrophil serine proteinase 4 (NSP4). These multifunctional proteinases are involved in the destruction of pathogens and in the regulation of inflammatory processes [1-3]. They act in combination with reactive oxygen species to degrade microorganisms engulfed inside phagolysosomes [4]. During phagocytosis and neutrophil turnover, NSPs are released in the extracellular space either free or bound to the membrane surface [5, 6].

NSPs are known to play pathogenic roles in chronic inflammatory diseases including chronic obstructive pulmonary disease (COPD) and auto-immune diseases such as granulomatosis with polyangiitis (GPA) [3, 7-9]. Human PR3 (hPR3) has been identified as the main target auto-antigen in GPA [10]. The interaction of auto-antibodies with membrane-bound hPR3 at the neutrophil surface induces cell activation and subsequent release of NETs, reactive oxygen species and proteinases [11, 12]. Progressive and destructive multifactorial lung diseases (COPD) and systemic small-vessel vasculitis (GPA) are associated with prolonged neutrophilic inflammation. Excessive activation of neutrophils liberating huge amounts of active serine proteinase in the extracellular medium initiates and promotes inflammatory tissue injury [3, 7-9].

hPR3 and its closest homologue hNE share a similar proteolytic specificity that has been deeply investigated using chromogenic and fluorogenic synthetic substrates [3, 13-15]. Both cleave substrates preferentially after small aliphatic residues (alanine, valine, aminobutyric acid, norvaline) [3, 14, 15]. The most significant structural difference in their substrate-binding pockets concerns the S2 subsite [16, 17]. The presence of a solvent-accessible Lys at position 99 makes the S2 subsite of hPR3 deeper and more polar than that of hNE, favoring accommodation of negatively charged or polar residues at P2 position [18]. In contrast, the substitution of Lys by Leu at position 99 provides a hydrophobic character to the S2 subsite of hNE that preferentially accommodates hydrophobic residues at P2 [14]. This makes Lys^{99} a key determinant to delineate the substrate specificity of hPR3.

In physiological conditions NSPs activities are regulated by different control mechanisms. They are expressed as inactive zymogens that require proteolytic processing and maturation during neutrophilic differentiation [9, 19]. At the inflammatory sites, the proteolytic activity of secreted NSPs is mainly controlled by the endogenous protein inhibitors, belonging to the serpin family (e.g. α1-proteinase inhibitor (α1-PI)), monocyte neutrophil elastase inhibitor (MNEI)) and chelonianins (SLPI, elafin) in the extracellular and pericellular space [3, 14, 15]. In normal conditions, the large excess of NSPs inhibitors prevents an unwanted degradation of connective tissue proteins such as elastin, collagen, and proteoglycans [20]. None of physiological proteinase inhibitors identified so far preferentially targets hPR3 in biological fluids or tissues. The main circulating serine proteinase

inhibitor, α1-PI, inhibits hPR3 at a much slower rate than hNE which raises the question of the control of hPR3 activity *in vivo* [21]. Recent data suggest and support an involvement of hPR3 more than hNE in the pathophysiology of COPD characterized with an imbalance between proteinases and inhibitors in the lung [22, 23]. Such an imbalance in the α1-PI/ proteinase ratio has been also reported as a risk for the development of GPA [24]. Moreover, the altered conformation of membrane-bound hPR3 at the surface of neutrophils makes it hardly inhibited and removed from the neutrophil surfaceby circulating α1-PI [25]. This probably contributes to its involvement as an auto-antigen in GPA.

NSPs, as a variety of proteinases belonging to all four major classes of proteinases, are also inhibited by the polyvalent inhibitor α2-macroglobulin (α2-M) [26]. α2-M is an abundant (2 mg/mL (12 µM)) glycosylated 725-kDa tetrameric plasma endoproteinase inhibitor synthesized in the liver [27-29]. This makes it the second circulating proteinase inhibitor in terms of blood molar concentration. Further it shows little variation with age [30]. α2-M enters the lungs by passive diffusion and its concentration is increased during inflammation. In human, α2-M exists as a homo-tetramer formed by non-covalent assembly of two dimers. Each dimer is composed of a pair of identical subunits containing 1451 residues (subunit size 180 kDa) linked by disulfide bridges [27, 31]. Marrero et al. demonstrated that α2-M operated through a unique irreversible "*venus flytrap*" mechanism, which entraps target proteinases in the inhibitor tetramer [32]. Proteinases are captured and trapped immediately by conformational changes occurring after the cleavage of a multitarget "39-residue bait region" (Pro^{690}-Thr^{728}) which is a pseudo-substrate containing specific sites for all target proteinases [27, 33]. The high rate of α2-M~proteinase formation relies on rapid processing of the bait region. In contrast to other inhibitors, the proteinase trapped within the α2-M is still accessible to small substrates and inhibitors, while being prevented from reaching insoluble fiber-forming substrates.

Virca et al. reported that the first step of hNE and hCatG inactivation consisted in the cleavage within the bait region of a 180 kDa α2-M subunit, into two fragments of ≈95 kDa and ≈85 kDa [33]. Cleavage sites by hNE and hCatG have been identified at expected bonds (Val^{711}-His^{712} for hNE and Phe^{697}-Tyr^{698} for hCatG). However, no cleavage site by hPR3 has been identified so far and no hPR3-sensitive site within the α2-M bait region can be deduced from previous studies on the structural determinants of hPR3 substrate specificity [3, 13-15]. In contrast to this observation however, similar association rate constants (k_{ass}) in the 10^7 $M^{-1}.s^{-1}$ range were reported for hNE and hPR3 [34]. To further investigate the role of α2-M as a physiological inhibitor of hPR3, we first characterized the neutralization of hPR3 by α2-M and predicted the putative hPR3-cleavage sites within the α2-M bait region using kinetic and molecular modeling approaches. We then identified the cleavage site of hPR3 in the 39-residue bait region of α2-M by mass spectrometry (MS).

RESULTS

Processing of α2-M by hPR3

The incubation of α2-M (1 µM) with hPR3 (0.1 and 0.5 µM) resulted in the processing of the 180-kDa monomer in two major fragments of about ~90 kDa (**Figure 1A**) as observed with hNE and hCatG in the same experimental conditions (**supp. Figure 1**). This cleavage resulted in the trapping of these proteinases within α2-M as controlled by ELISA, checking the absence of recognition of the trapped proteinase by the monoclonal anti-hPR3 antibody Ab CLB12.8 (*not shown*). The processing of α2-M bait region however was far slower than that observed using hNE (**supp. Figure 1**).

Prediction of hPR3 cleavage sites in the bait-region segment of α2-M

On the basis of the known S1 specificity of hPR3 at least eight putative cleavage sites in the bait-region of α2-M can be identified, namely Met^{697}, Val^{705}, Ser^{710}, Val^{712}, Met^{713}, Ala^{718}, Val^{721}, Val^{723} with Val and Ala being the preferential P1 residues for both hPR3 and hNE (**Figure 1B, C, D**). Three of these predicted P1 residues are preceded by a negatively charged residue (Glu^{696}, Glu^{709}, Asp^{711}), which is a discriminant feature to define hPR3 specificity. Of these, only Val^{712} is predicted to have significant cleavage. However, the presence at P3 of a serine residue (Ser^{710}) compromises the cleavage after Val^{712} [35]. This means that there is no peptide bond within the α2-M bait region, which clearly appears as a highly sensitive predicted cleavage site for hPR3, based on its reported substrate specificity. Other putative cleavage sites with Ala or Val at P1 possess leucyl or histidyl residues at P2 (---**His**^{717}-Ala^{718}-**Leu**^{720}-Val^{721}-**His**^{722}-Val^{723}---) with an histidyl that may be partially protonated and has never been identified in any protein/peptide substrate sequence cleaved by hPR3.

Non-preferential cleavages of sequences containing a hydrophobic residue such as Leu/Ile at P2 position by hPR3 unlike hNE were observed by analysis of the cleavage sites in melittin and insulin B chain (**Figure 2, supp. Figure 2 and 3** and **supp. Table1**). Since **Leu**^{11}-Val^{12} and **Leu**^{17}-Val^{18} were slowly cleaved in the B chain of oxidized insulin, we decided to test the influence Leu at P2 by introducing this residue in hPR3 synthetic substrates. Similarly, we decided to test the influence of a His in P2.

Influence of histidine and leucine at P2 on the catalytic activity of hPR3

As shown in Table 1, the reference substrates with an Asp in P2, i.e. substrate **1** ABZ-VA**D**(nor)VADYQ-EDDnp (substrate **1),** Biotin-PY**D**(nor)V-AMC (substrate **9),** have a k_{cat}/K_m of 7000 $M^{-1}.s^{-1}$ [18] and 468 $M^{-1}.s^{-1}$, respectively. A P2 His in ABZ-VA**H**(nor)VADYQ-EDDnp (substrate **2**) and P2 Leu in ABZ-VA**L(**nor)VADYQ-EDDnp (substrate **3**) decreased the specificity constant k_{cat}/K_m for PR3 by a factor of ~100 (76 $M^{-1}.s^{-1}$ *vs* 7000 $M^{-1}.s^{-1}$) and ~10 (503 $M^{-1}.s^{-1}$ *vs* 7000 $M^{-1}.s^{-1}$), respectively (**Table 1**), without altering the K_m value (~1 µM). ABZ-VA**H**(nor)VADYQ-

EDDnp (substrate **2**) was cleaved between **(**nor)Val and Ala as expected, but two cleavage sites ((nor)Val-Ala and Ala-Asp) were identified in ABZ-VA**L**(nor)VADYQ-EDDnp (substrate **3**) (**Figure 3**). Further ABZ-VA**L**(nor)VADYQ-EDDnp (substrate **3**) was cleaved at the (nor)Val-Ala bond by hNE (k_{cat}/K_m = 81 $M^{-1}.s^{-1}$) while ABZ-VA**H**(nor)VADYQ-EDDnp resisted cleavage by hNE, as did the parent substrate (**Table 1**). P2 His in Biotin-PY**H**(nor)V-AMC (substrate **10**) and P2 Leu Biotin-PY**L**(nor)V-AMC (substrate **11**) decreased the specificity constant k_{cat}/K_m for hPR3 (36 $M^{-1}.s^{-1}$ *vs* 468 $M^{-1}.s^{-1}$; 34 $M^{-1}.s^{-1}$ *vs* 468 $M^{-1}.s^{-1}$) by ~15 (**Table 1**). For comparison Tyr, Pro, Thr, Trp and Arg residues were assessed at P2 position in ABZ-peptidyl-EDDnp substrates (substrates **4-8**). The k_{cat}/K_m value of the substrates with P2 His or Arg, for hPR3 were similar.

Computational docking analysis of P2 histidine and leucine interaction with hPR3

The computational docking approach employed here have revealed interactions between the ε-amino group of Lys^{99} with Biotin-Pro amide oxygen and P2 Asp side chain carboxyl moiety of Biotin-PY**D**(nor)V-AMC which are analogous to those described previously for PR3-phosphonic inhibitors binding models [36]. The key role for an efficient/effective substrate recognition and binding seems to play the interaction between the P2 residue side chain carboxyl with Lys^{99}. Its essential role is highlighted when P2 Asp residue is replaced by His or Leu yielding compounds with a significant drop of activity/susceptibility to PR3-mediated hydrolysis such as Biotin-PY**H**(nor)V-AMC and Biotin-PY**L**(nor)V-AMC. The models obtained for these P2-replaced substrates show that the side-chains at this position are shifted away from Lys^{99} towards the cavity that is present beyond this residue. As a consequence the whole backbone of the substrate is moved forward the catalytic center placing P3 and P4 substrate residues in new molecular environment (**Figure 4**). As the obtained models represent a theoretical prediction of substrates-enzyme binding while/but since hPR3 shows no significant activity towards sequences with P2 His and Leu, the true binding is highly questionable to take place. It may suggested that the cavity present beside the S2 pocket does not participate in substrate binding and the P2 position specificity depends mainly on the interaction with Lys^{99}.

The kinetic and docking data confirmed that Leu-Val^{721}-His^{722} could be relatively slowly cleaved by hPR3 in the bait-region sequence of α2-M. We used the complete 39-residue peptide of the bait region as a substrate to identify the cleavage sites by both hPR3 and hNE.

Identification of hPR3 cleavage sites in the α2-M bait region sequence by mass spectrometry

To assess the sensitivity of whole α2-M to hPR3 in the bait region according to the above predictions, cleavage products of α2-M at two different time points were identified by MS analysis (**Figure S4**). While cleavages were observed within the bait region as well as upstream of it (**Figure S4A)**, the majority of α2-M proteins remained intact or slightly shortened in the presence of hPR3 (**Figure S4B)**. Although some variation in cleavage intensities can be seen (**Figure 5**), no

hypersensitive site was found in α2-M. On the other hand, incubation of the 39-residue bait region peptide (39pep-α2-M) with hPR3 resulted in a major cleavage at Leu^{720}-Val^{721} ↓ His^{722} (α2-M numbering) as observed by HPLC and MS analysis (**Figure 6A**). This site corresponds to that reported using hNE [33]. Three minor cleavages were observed at Glu^{709}-Ser^{710}↓ Asp^{711}, Val^{712}-Met^{713}↓ Gly^{714}, His^{717}-Ala^{718} ↓ Arg^{719}. Indeed, we confirmed that hNE cleaved 39pep-α2-M far more rapidly than did hPR3. An additional cleavage by hNE was identified at Arg^{704}-Val^{705} ↓ Gly^{706} which was fairly resistant to cleavage by hPR3 (**Figure 6B** and **Supp. Figure 5**). To further examine the cleavage propensity of secondary sites by hPR3 in the α2-M bait region, we developed the fluorogenic substrate ABZ-GRGHARLVHVEEPHT-Y_{NO2} (substrate **12**) derived from the C-terminally-cleaved region of 39pep-α2-M and compared the specificity constants for hPR3 and hNE. MS analysis confirmed that the substrate was cleaved at the Val-His bond for both proteinases, and kinetic analysis showed that the cleavage by hNE was about 40 times more efficient than that by hPR3 in the same experimental conditions (k_{cat}/K_m = 1575 $M^{-1}.s^{-1}$ *vs* 35 $M^{-1}.s^{-1}$). The substrate ABZ-GFYESDVMGRG-Y_{NO2} (substrate **13**) which also contains part of the α2-M bait region sequence was very slowly hydrolyzed at several sites by hPR3 (k_{cat}/K_m < 2 $M^{-1}.s^{-1}$) but not by hNE (**Table 2**).

DISCUSSION

NSPs have evolved specificities that make them precise and efficient actors in a number of pathophysiological functions [3, 37]. The proteolytic activity of NSPs is regulated under physiological conditions by natural inhibitors present at the inflammatory site [3, 15, 38]. Most of them circulate in the bloodstream, especially the members of the serpin family including α1-PI, ACT, that represent about 10% of the blood proteins, and α2-M. Though α1-PI preferentially inhibits hNE, has a high circulating concentration of 1 to 2 mg/mL (~30 µM), and is the major physiological inhibitor of hPR3, [39]. Its concentration increases during the acute phase of inflammation, but it interacts slowly enough with hPR3 to inhibit almost the total hNE present in the milieu before starting to inhibit hPR3 [40]. α1-PI act as a "suicide" substrate, a type of inhibitor thus named because the attack on the peptide bond by target proteinases leads to the bond cleavage as well as the formation of an inactive and pseudo-irreversible proteinase-inhibitor complex [41]. The rate constant of association between α1-PI and hNE is 1.4 × 10^7 $M^{-1}.s^{-1}$, which is ~20 fold higher than that determined with hPR3 (k_{ass} = 4.5 × 10^5 $M^{-1}.s^{-1}$ [13], k_{ass} = 9.2 × 10^6 $M^{-1}.s^{-1}$ [22]).

This raises the question whether the other major circulating inhibitor, i.e. α2-M, is capable of supplementing α1-PI for the control of hPR3 activity in normal or inflammatory conditions. α2-M is a large protein inhibiting proteinases of several classes that is also abundant in the plasma [33]. α2-M inhibits target proteinases in two steps, first cleaving the bait region then entrapping the proteinase, a

mechanism that impairs access of large protein substrates to the active site of the entrapped proteinase [32]. The cleavage site of hNE in the bait-region has been identified by Virca et al. as Leu-Val^{721} ↓ His^{722} [33]. Rao et al. reported that hPR3 was inhibited by α2-M and determined the association constant k_{ass} as 10^7 $M^{-1}.s^{-1}$. On the basis of the known P4-P2' specificity of hPR3 deduced from previous structural and kinetics studies the α2-M bait region sequence should be poorly cleaved by hPR3 [3, 13, 14, 25, 36, 42, 43]. Using kinetic and molecular modeling analysis, we have further investigated the cleavable sequences of α2-M bait region by hPR3, with the aim to clarify whether α2-M can play a significant role as a potential physiological inhibitor of hPR3.

The S1/P1 specificity of hPR3 and related-serine proteinases confers to these proteinases their specificity of cleavage. The S1 subsite of hPR3 is hemispherical but is smaller than that of hNE due to the substitution of the valine residue for an isoleucine at position 190 [16]. Both hPR3 and hNE preferentially accommodate small hydrophobic residues such as valine, cysteine, alanine at the P1 position. However, the S2/P2 specificity of hPR3 is essential to discriminate between hPR3 and hNE [18]. The substitution of Leu^{99} in hNE by a lysine in hPR3 is the key structural determinant clarifying why hPR3 preferentially accommodates a negative or polar residue at P2 [13, 14]. At this position, hNE accommodates hydrophobic residues due to the presence of Leu^{99} [13, 14]. On the basis of the known S4-S2' specificity of hPR3 and of the observed cleavage sites in melittin and insulin B chain, the sequences Gly-**His**-Ala^{718}-Arg^{719} and Arg-**Leu**-Val^{721}-His^{722} with a His and Leu at P2, respectively, were predicted as possible hPR3 cleavable sequences in the α2-M bait region.

While His was not found at P2 in natural hPR3 substrates, combinatorial chemistry- or phage displays-identified synthetic hPR3 substrates [3, 13-15, 44], hydrophobic Leu would not be preferentially accommodated by hPR3 due to the hydrophilic characteristic of its S2 pocket [3, 13, 14, 16]. Moreover, the FRET substrate derived from protein C inhibitor ABZ-IFTFRSA/RLNSQRLV/FNRQ-EDDnp was cleaved by hPR3 and hNE at Arg-**Ser**-Ala ↓ Arg and Arg-**Leu**-Val ↓ Phe, respectively [13]. All data suggested that hNE cleavable sequence in the α2-M bait region Arg-**Leu**-Val^{721}-His^{722} was not a hPR3-sensitive site. We have therefore assessed the influence of His and Leu at P2 by introducing these residues in hPR3 synthetic fluorogenic substrates. The substitution of the P2 Asp preferentially accommodated by hPR3 at this position by His or Leu significantly decreases the rate of hydrolysis. The natural peptides melittin and oxidized insulin B−chain [45, 46] or peptides were rapidly cleaved by hPR3 after small hydrophobic residues Ala, Val, preceded by a negatively charged or a hydrophilic residue (which were very slowly cleaved by hNE). However, the sequences containing hydrophobic Leu or Ile at P2 position were more slowly cleaved by hPR3 even if the P1 residue was a Val or an Ala. These sequences were more rapidly cleaved by hNE, confirming that the P2 residue provides proteolytic specificity to hPR3 and hNE.

The analysis of hPR3 structure revealed that in close proximity to the Lys^{99} of S2, a quite spacious cavity that potentially could accommodate residues bulkier than Asp such as Leu or His is

present [16]. Computational docking of the substrates Biotin-PY**D**(nor)V-AMC, Biotin-PY**H**(nor)V-AMC and Biotin-PY**L**(nor)V-AMC in the hPR3 active site showed a general binding pose similar to the model obtained previously for the phosphonate inhibitors [36]. In the model of the optimal substrate Biotin-PY**D**(nor)V-AMC, the crucial interactions of Lys^{99} with substrate P2 Asp carboxyl group and Biotin-Pro amide are observed. For the models of substrates bearing Leu or His as P2 residues, the side-chain is moved away from Lys^{99} towards catalytic His^{57} and Asp^{102}. Therefore, not only do the electrostatic interactions/hydrogen bonding generated by Lys^{99} play an important role for recognition and binding of the substrate, but also the repulsive effect on more hydrophobic residues at P2 may negatively affect the catalytic triad environment and function.

Finally, we analyzed the processing of whole α2-M by hPR3 by MS to test for sensitivity in the bait region. At a low enzyme:substrate ratio of 1:2250, no cleavage of α2-M was observed (data not shown). At 1:225 ratio, the majority of the α2-M protein pool remained unprocessed. Though a reduction step was applied to break disulfide bridges to ensure that cleavage products were released from the protein, only low intensity cleavage products appeared in the lower mass region. Most of the cleavages were observed in the bait region sequence and were consistent with the predicted cleavage sites. To compare the relative sensitivities of cleavage of α2-M by hNE *versus* hPR3, we analyzed the processing of the 39-residue peptide corresponding to the bait region. HPLC and MS analysis revealed that the major cleavage site of hPR3 was Leu^{720}-Val^{721} ↓ His^{722}, corresponding to one of the two hNE sites previously reported by Virca et al. [33]. 39pep-α2-M and the FRET substrate containing the cleavage site were more rapidly cleaved by hNE. We identified an additional cleavage site by hNE **Arg**-Val^{705} ↓ Gly^{706} at the N-terminus of 39pep-α2-M. Arg is not well accommodated at P2 position by hPR3 due to the S2-pocket Lys^{99} [18, 42]. The presence of a P2 Arg makes this sequence resistant to cleavage by hPR3. The 39-residue peptide was poorly and slowly cleaved by hPR3. Altogether with the whole-protein sensitivity analysis, these results suggest that α2-M is not an efficient inhibitor of hPR3, which was confirmed by the estimation of k_{ass} between α2-M and hPR3 in the $\leq 10^5\ M^{-1}s^{-1}$ range.

With this current work, we completed the study on physiological inhibitors of hPR3 and showed that this proteinase is the least controlled NSP. The consequences are that there may be pathological conditions where hPR3 is the only NSPs that remains active and can alone cause proteolytic damage. It is consistent with the presence of active hPR3 and significantly greater than hNE activity in lung secretions from patients suffering from α1-PI deficiency, a genetic disorder associated with early onset COPD [23]. Sinden et al. highlighted a potentially important pathologic role for hPR3 in α1-PI deficiency because of its reduced association rate constant with α1-PI variants as well as with wild type α1-PI [22]. In this pathological condition, local α2-M concentrations mainly regulate NSPs [22]. Poor inhibition of hPR3 by α2-M would increase its pro-inflammatory and tissue injury effects. This helps to explain the potential role of hPR3 in inflammation and its unique role in GPA, coming to the point of developing synthetic inhibitors that specifically target this proteinase.

We conclude that hPR3 and hNE have different interaction with endogenous inhibitors, which is true for α2-M. Knowledge of structural and functional differences between these homologous proteinases is crucial for the interpretation of their individual function in the regulation of inflammatory process. The poor inhibition of hPR3 by endogenous inhibitors points out its involvement in tissue injury during chronic inflammatory diseases such as COPD and its known function as major target auto-antigen in GPA. Such an insight opens the space for the development of highly selective hPR3 inhibitors which simultaneously are inactive towards other members of the NSP family. The already developed synthetic low molecular weight inhibitors of hPR3 such as Bt-Pro-Tyr-Asp-Ala^{p}(O-C_6H_4-4-Cl)$_2$ or Bt-Val-Tyr-Asp-(nor)Val^{p}(O-C_6H_4-4-Cl)$_2$ (25,36) might fill the gap in the lack of availability of selective hPR3-directed GAP-associated inflammation reducers. Althoug much of work is still ahead, the fundaments required for reasonable design of selective inhibitors makes this challenge possible to undertake with a successful outcome.

MATERIALS AND METHODS

***Materials*-** Human recombinant α2-M (10952-H08B) and human plasma α2-M (SRP6314-1) were obtained from Sino Biological and Sigma Aldrich (St-Louis, MO, USA) and Athens Research & Technology (Athens, GA, USA). hNE (EC 3.4.21.37) was provided by Athens Research & Technology (Athens, GA, USA). The oxidized insulin B-chain and melittin were from Sigma-Aldrich (St-Louis, MO, USA). The 39pep-α2-M and fluorogenic substrates Biotin-PYD(nor)V-AMC, Biotin-PYH(nor)V-AMC, Biotin-PYL(nor)V-AMC, ABZ-VAR(nor)VADYQ-EDDnp ABZ-GFYESDVMGRG-Y_{NO2}, and ABZ-GRGHARLVHVEEPHT-Y_{NO2}, were synthesized by Genecust (Dudelange Luxembourg). IGEPAL® CA-630 (NP40) was purchased from Sigma-Aldrich (St. Louis, MO, USA). Recombinant hPR3 (EC 3.4.21.76) was produced and activated as in [35]. Proteolysis of mellitin and insulin B-chain were performed using hPR3 from Dr. P. Davies and Dr J.L. Humes.

***Electrophoresis*-** A solution of α2-M at 1 μM was incubated with or without 0.1 and 0.5 μM hPR3 for 10-120 min at 37 °C in PBS (Phosphate Buffered Saline) solution (1X, pH 7.4). The mixtures were then denatured/reduced by addition of reducing buffer (1X, β-mercaptoethanol) and then boiled during 5 min at 100 °C. The mixtures were separated on a 10% SDS-PAGE gel at room temperature at constant amperage of 25 mA per gel for about 1 h and visualized by silver nitrate (Invitrogen) staining according to the manifacturer's protocol. Size markers (10 to 250 kDa) used was PageRuler Plus Prestained Protein Ladder, (Thermo Fisher Scientific, Waltham, MA, USA). The bands representing the proteins according to their size appeared dark brown on the gel.

***ELISA*-** hPR3 (ab153798, Abcam, Paris, France) and hPR3 (34 nM - 1.72 nM) previously incubated with α2-M (6.09 nM) (ref.10952-H08B, Sino Biological) at 37 °C for 1 h were used in a capture ELISA with precoated nickelchelate microtiter 96-well plates (Thermo Fisher Scientific). 100 μL of samples diluted in PBS-Tween 20 at 0.05% buffer were incubated at room temperature for 16 h. After washing three times each well with 200 μL of PBS-Tween 20 at 0.05%, 100 μL of mouse monoclonal antibody anti-hPR3 antibody CLB 12.8 (Sanquin, Amsterdam, The Netherlands) diluted at 1:1000 in PBS-Tween 20 at 0.05% buffer was added on each sample and incubated at room temperature for 1 h. After a new cycle of three washes, 100 μL of human IgG polyclonal antibody anti-Fc (ref A2290, Sigma Aldrich, (St-Louis, MO, USA) diluted at 1:300 in PBS-Tween 20 at 0.05 % buffer were added, and then incubated for 1 h. Ortho-phenylenediamine (P9187, Sigma Aldrich) and H_2O_2 were then added for 20 minutes. H_2SO_4 stop solution was then added. Absorbances were read spectrophotometrically (Spectramax Gemini, Molecular Devices, Sunnyvale, CA, USA)) at 492 nm.

k_{cat}/K_m and K_m determination by spectrofluorimetry- The specificity constant (k_{cat}/K_m) and the Michaelis constant (K_m) for fluorogenic substrates were determined under pseudo first-order conditions [47]. The cleavage of the substrates at a final concentration of 1 µM at 37 °C in cleavage buffer (50 mM HEPES, 0.75 M NaCl, 0.05% NP40, pH 7.4), was monitored on a Spectramax Gemini (Molecular Devices, Sunnyvale, CA, USA) (with excitation/emission wavelengths: 320 nm/420 nm (FRET substrates); 350 nm/460 nm (AMC substrates). Final proteinase concentrations were 0.001-2 µM.

Proteolysis for cleavage sites identification- 39pep-α2-M (50 µM final) was incubated with hPR3 (5.10^{-8} M) or hNE (10^{-9} M) at 37 °C for 3 h in PBS. FRET substrates (20 µM final) were incubated with hPR3 or hNE lysate supernatant (0.001-2 µM) at 37 °C in cleavage buffer. A solution of α2-M at 16 µM was incubated with or without 0.5 µM hPR3 (1:225 enzyme:substrate ratio w/w) for 1 h at 37 °C in incubation buffer consisting of 100 mM ammonium bicarbonate pH 8.5, 700 mM NaCl and 0.05% NP40. A control with hPR3 alone was performed. For melittin and oxidized insulin B chain, assays were performed in a total volume of reaction of 20 µL. hPR3 and hNE at a final concentration of 0.835 µM was reacted with melittin (715 µM) or insulin B-chain (570 µM) in 200 mM Tris-acetate, pH 7.4, at 23 °C. On the basis of ponderal concentrations, the substrate was in a ~80-fold excess over the proteinase

Chromatographic procedures- For the 39pep-α2-M and FRET substrates, following proteolysis the proteinases were precipitated with absolute ethanol (4 volumes). The supernatant containing the peptides were dried under vacuum and dissolved in 200 µL of 0.01% trifluoroacetic acid (v/v), then fractionated by Agilent Technology 1200 Series HPLC system (Agilent Technology, CA, USA) on a C18 column (2,1×30 mm, Merck Millipore) at a flow rate of 0.3 mL/min with a linear gradient (0-90%, v/v) of acetonitrile in 0.01% trifluoroacetic acid over 40 min. Eluted peaks were monitored at 220 and 360 nm.

Mass spectrometry- LC-MS. For melittin and oxidized insulin B chain, the incubation medium at t = 95 min (20 µL) was quenched by a 6-fold dilution into 1% aqueous TFA. The cleavage products were separated by RP-HPLC on a 2.1 x 250 mm Vydac C18 column (MW-Analysen-Technik, Germany) connected to 140A HPLC device (Applied Biosystems, Foster City, USA). A 120 min linear gradient from 2 to 60% acetonitrile in 0.05% aqueous TFA was applied at a flow rate of 0.25 mL/min. Post-column splitting of the flow was achieved via a stainless Valco tee. Approximately $1/15^{th}$ of the effluent was directed to the mass spectrometer by means of a fused silica capillary with an internal diameter of 75 µm, while the remaining effluent was analyzed by UV-detection at 214 nm and collected for further MALDI-TOF MS analysis. The online analysis was performed using a Bio-Q electrospray triple-quadrupole mass spectrometer (ESI-TQ MS) from VG BioTech (Manchester UK). Scans were acquired in positive ion mode at 0.2 Hz in the 500 to 2000 *m/z* range. The instrument was calibrated using horse heart myoglobin at 2 µM in a 49:50:1 water:acetonitrile:formic acid solution.

MALDI-TOF MS. For melittin and oxidized insulin B chain, a 1 µL aliquot was withdrawn from the reaction medium at different time points and diluted to quench the enzymatic reaction prior to analysis in 50 µL of 0.1% aqueous TFA. The MALDI sample spots were prepared as follows: 1 µL of saturated 4-hydroxy-α-cyano-cinnamic acid (4HCCA) solution in acetone was deposited on the stainless steel probe and allowed to quickly evaporate. About 0.5 µL of proteolysis product solution was then deposited on top of the matrix surface and allowed to air-dry. Last, the sample was washed with 0.5% aqueous TFA. Mass spectra were obtained using a Bruker (Bremen, Germany) Biflex MALDI-TOF mass spectrometer. The instrument was operated in the linear positive ion mode. The instrument was calibrated with a standard mixture of angiotentin II, ACTH 18-39 and bovine insulin. The instrument control and data processing were done with the Bruker built-in software on a Sun Sparc workstation.

39pep-α2-M and α2-M samples were analyzed on an UltraFlex I mass spectrometer (Bruker Daltonics). A cysteine reduction was carried out for 10 min at 37 °C using 5 mM Tris(2-carboxyethyl)phosphine hydrochloride prior to MS analysis of whole α2-M samples. Samples were diluted fifty-fold or hundred-fold in a solution of 4HCCA saturated in a solution of 66.6% water, 33.3% acetonitrile, and 0.1% trifluoroacetic acid. Matrix-sample solutions were spotted onto a gold-plated sample probe using the ultrathin layer method [48, 49]. Spectra were acquired in linear positive ion mode for α2-M samples and in reflectron positive ion mode for 39pep-α2-M samples. Calibration of the instrument was performed externally using a neighboring spot with protein calibration mix consisting of apomyoglobin and cytochrome c or with pepmix I from Bruker. MALDI-TOF-MS spectra were processed and annotated using FlexAnalysis 3.3 (Bruker Daltonics) and PAWS 8.5 (ProteoMetrics) software, respectively.

Molecular docking- The *in silico* analysis of protein-ligand binding mode was performed with the crystal structure of hPR3 used as a receptor (1FUJ.pdb) [16]. The models of ligands structure were prepared and optimized using ChemBio3D 12.0 with MM2 force field [50]. The protonation and atom types of all molecules were set with SPORES [51]. Docking studies were performed using Protein-Ligand ANT System (PLANTS v. 1.2) [52-54]. The simulations were carried out with the enzyme binding site defined as described before [36]. The distance constrains were defined in a similar fashion as in previous study with the exception of interactions inside the S2 binding site as it was the position of interest in current studies. The constrains included (a) the distance between the hydroxide oxygen of catalytic serine residue and norVal carbonyl carbon of the substrate (distance range was set between 2.2 and 4.0 Å); (b) Ile^{190} γ-carbon located at the bottom of S1 pocket and terminal carbon of norVal side chain (distance range: 2.2-5.0 Å) and (c) Val^{216} carbonyl oxygen of hPR3 and nitrogen of the substrate P3-P4 amide bond.

REFERENCES

1. Pham, C. T. (2006) Neutrophil serine proteases: specific regulators of inflammation, *Nat Rev Immunol.* **6**, 541-50.

2. Pham, C. T. (2008) Neutrophil serine proteases fine-tune the inflammatory response, *Int J Biochem Cell Biol.* **40**, 1317-33.

3. Korkmaz, B., Horwitz, M., Jenne, D. E. & Gauthier, F. (2010) Neutrophil elastase, proteinase 3 and cathepsin G as therapeutic targets in human diseases, *Pharmacol Rev.* **62**, 726-59.

4. Segal, A. W. (2005) How neutrophils kill microbes, *Annu Rev Immunol.* **23**, 197-223.

5. Campbell, E. J. & Owen, C. A. (2007) The sulfate groups of chondroitin sulfate- and heparan sulfate-containing proteoglycans in neutrophil plasma membranes are novel binding sites for human leukocyte elastase and cathepsin G, *J Biol Chem.* **282**, 14645-54.

6. Korkmaz, B., Jaillet, J., Jourdan, M. L., Gauthier, A., Gauthier, F. & Attucci, S. (2009) Catalytic activity and inhibition of wegener antigen proteinase 3 on the cell surface of human polymorphonuclear neutrophils, *J Biol Chem.* **284**, 19896-902.

7. Schonermarck, U., Csernok, E. & Gross, W. L. (2015) Pathogenesis of anti-neutrophil cytoplasmic antibody-associated vasculitis: challenges and solutions 2014, *Nephrol Dial Transplant.* **30 Suppl 1**, i46-52.

8. Crisford, H., Sapey, E. & Stockley, R. A. (2018) Proteinase 3; a potential target in chronic obstructive pulmonary disease and other chronic inflammatory diseases, *Respir Res.* **19**, 180.

9. Korkmaz, B., Caughey, G. H., Chapple, I., Gauthier, F., Hirschfeld, J., Jenne, D. E., Kettritz, R., Lalmanach, G., Lamort, A. S., Lauritzen, C., Legowska, M., Lesner, A., Marchand-Adam, S., McKaig, S. J., Moss, C., Pedersen, J., Roberts, H., Schreiber, A., Seren, S. & Thakker, N. S. (2018) Therapeutic targeting of cathepsin C: from pathophysiology to treatment, *Pharmacol Ther.* **190**, 202-236.

10. Jenne, D. E., Tschopp, J., Ludemann, J., Utecht, B. & Gross, W. L. (1990) Wegener's autoantigen decoded, *Nature.* **346**, 520.

11. Kettritz, R. (2012) How anti-neutrophil cytoplasmic autoantibodies activate neutrophils, *Clin Exp Immunol.* **169**, 220-8.

12. Kettritz, R. (2016) Neutral serine proteases of neutrophils, *Immunol Rev.* **273**, 232-48.

13. Korkmaz, B., Kellenberger, C., Viaud-Massuard, M. C. & Gauthier, F. (2013) Selective inhibitors of human neutrophil proteinase 3, *Curr Pharm Des.* **19**, 966-76.

14. Korkmaz, B., Lesner, A., Guarino, C., Wysocka, M., Kellenberger, C., Watier, H., Specks, U., Gauthier, F. & Jenne, D. E. (2016) Inhibitors and Antibody Fragments as Potential Anti-Inflammatory Therapeutics Targeting Neutrophil Proteinase 3 in Human Disease, *Pharmacol Rev.* **68**, 603-30.

15. Korkmaz, B., Moreau, T. & Gauthier, F. (2008) Neutrophil elastase, proteinase 3 and cathepsin G: physicochemical properties, activity and physiopathological functions, *Biochimie.* **90**, 227-42.

16. Fujinaga, M., Chernaia, M. M., Halenbeck, R., Koths, K. & James, M. N. (1996) The crystal structure of PR3, a neutrophil serine proteinase antigen of Wegener's granulomatosis antibodies, *J Mol Biol.* **261**, 267-78.

17. Bode, W., Wei, A. Z., Huber, R., Meyer, E., Travis, J. & Neumann, S. (1986) X-ray crystal structure of the complex of human leukocyte elastase (PMN elastase) and the third domain of the turkey ovomucoid inhibitor, *Embo J.* **5**, 2453-8.

18. Korkmaz, B., Hajjar, E., Kalupov, T., Reuter, N., Brillard-Bourdet, M., Moreau, T., Juliano, L. & Gauthier, F. (2007) Influence of charge distribution at the active site surface on the substrate specificity of human neutrophil protease 3 and elastase. A kinetic and molecular modeling analysis, *J Biol Chem.* **282**, 1989-97.

19. Adkison, A. M., Raptis, S. Z., Kelley, D. G. & Pham, C. T. (2002) Dipeptidyl peptidase I activates neutrophil-derived serine proteases and regulates the development of acute experimental arthritis, *J Clin Invest.* **109**, 363-71.

20. Janoff, A. (1985) Elastase in tissue injury, *Annu Rev Med.* **36**, 207-16.

21. Korkmaz, B., Attucci, S., Jourdan, M. L., Juliano, L. & Gauthier, F. (2005) Inhibition of neutrophil elastase by alpha1-protease inhibitor at the surface of human polymorphonuclear neutrophils, *J Immunol.* **175**, 3329-38.

22. Sinden, N. J., Baker, M. J., Smith, D. J., Kreft, J. U., Dafforn, T. R. & Stockley, R. A. (2015) alpha-1-antitrypsin variants and the proteinase/antiproteinase imbalance in chronic obstructive pulmonary disease, *Am J Physiol Lung Cell Mol Physiol.* **308**, L179-90.

23. Sinden, N. J. & Stockley, R. A. (2013) Proteinase 3 activity in sputum from subjects with alpha-1-antitrypsin deficiency and COPD, *Eur Respir J.* **41**, 1042-50.

24. Rooney, C. P., Taggart, C., Coakley, R., McElvaney, N. G. & O'Neill, S. J. (2001) Anti-proteinase 3 antibody activation of neutrophils can be inhibited by alpha1-antitrypsin, *Am J Respir Cell Mol Biol.* **24**, 747-54.

25. Guarino, C., Legowska, M., Epinette, C., Kellenberger, C., Dallet-Choisy, S., Sienczyk, M., Gabant, G., Cadene, M., Zoidakis, J., Vlahou, A., Wysocka, M., Marchand-Adam, S., Jenne, D. E., Lesner, A., Gauthier, F. & Korkmaz, B. (2014) New selective peptidyl di(chlorophenyl) phosphonate esters for visualizing and blocking neutrophil proteinase 3 in human diseases, *J Biol Chem.* **289**, 31777-91.

26. Rehman, A. A., Ahsan, H. & Khan, F. H. (2013) alpha-2-Macroglobulin: a physiological guardian, *J Cell Physiol.* **228**, 1665-75.

27. Sottrup-Jensen, L. (1989) Alpha-macroglobulins: structure, shape, and mechanism of proteinase complex formation, *J Biol Chem.* **264**, 11539-42.

28. Barrett, A. J. & Starkey, P. M. (1973) The interaction of alpha 2-macroglobulin with proteinases. Characteristics and specificity of the reaction, and a hypothesis concerning its molecular mechanism, *Biochem J.* **133**, 709-24.

29. Travis, J. & Salvesen, G. S. (1983) Human plasma proteinase inhibitors, *Annu Rev Biochem.* **52**, 655-709.

30. Petersen, C. M. (1993) Alpha 2-macroglobulin and pregnancy zone protein. Serum levels, alpha 2-macroglobulin receptors, cellular synthesis and aspects of function in relation to immunology, *Dan Med Bull.* **40**, 409-46.

31. Andersen, G. R., Koch, T. J., Dolmer, K., Sottrup-Jensen, L. & Nyborg, J. (1995) Low resolution X-ray structure of human methylamine-treated alpha 2-macroglobulin, *J Biol Chem.* **270**, 25133-41.

32. Marrero, A., Duquerroy, S., Trapani, S., Goulas, T., Guevara, T., Andersen, G. R., Navaza, J., Sottrup-Jensen, L. & Gomis-Ruth, F. X. (2012) The crystal structure of human alpha2-macroglobulin reveals a unique molecular cage, *Angew Chem Int Ed Engl.* **51**, 3340-4.

33. Virca, G. D., Salvesen, G. S. & Travis, J. (1983) Human neutrophil elastase and cathepsin G cleavage sites in the bait region of alpha 2-macroglobulin. Proposed structural limits of the bait region, *Hoppe Seylers Z Physiol Chem.* **364**, 1297-302.

34. Virca, G. D. & Travis, J. (1984) Kinetics of association of human proteinases with human alpha 2-macroglobulin, *J Biol Chem.* **259**, 8870-4.

35. Jegot, G., Derache, C., Castella, S., Lahouassa, H., Pitois, E., Jourdan, M. L., Remold-O'Donnell, E., Kellenberger, C., Gauthier, F. & Korkmaz, B. (2011) A substrate-based approach to convert SerpinB1 into a specific inhibitor of proteinase 3, the Wegener's granulomatosis autoantigen, *FASEB J.* **25**, 3019-31.

36. Guarino, C., Gruba, N., Grzywa, R., Dyguda-Kazimierowicz, E., Hamon, Y., Legowska, M., Skorenski, M., Dallet-Choisy, S., Marchand-Adam, S., Kellenberger, C., Jenne, D. E., Sienczyk, M., Lesner, A., Gauthier, F. & Korkmaz, B. (2018) Exploiting the S4-S5 Specificity of Human Neutrophil Proteinase 3 to Improve the Potency of Peptidyl Di(chlorophenyl)-phosphonate Ester Inhibitors: A Kinetic and Molecular Modeling Analysis, *J Med Chem.* **61**, 1858-1870.

37. Perera, N. C., Schilling, O., Kittel, H., Back, W., Kremmer, E. & Jenne, D. E. (2012) NSP4, an elastase-related protease in human neutrophils with arginine specificity, *Proc Natl Acad Sci U S A.* **109**, 6229-34.

38. Perera, N. C., Wiesmuller, K. H., Larsen, M. T., Schacher, B., Eickholz, P., Borregaard, N. & Jenne, D. E. (2013) NSP4 is stored in azurophil granules and released by activated neutrophils as active endoprotease with restricted specificity, *J Immunol.* **191**, 2700-7.

39. Hollander, C., Westin, U., Wallmark, A., Piitulainen, E., Sveger, T. & Janciauskiene, S. M. (2007) Plasma levels of alpha1-antichymotrypsin and secretory leukocyte proteinase inhibitor in healthy and chronic obstructive pulmonary disease (COPD) subjects with and without severe alpha1-antitrypsin deficiency, *BMC Pulm Med.* **7**, 1.

40. Korkmaz, B., Poutrain, P., Hazouard, E., de Monte, M., Attucci, S. & Gauthier, F. L. (2005) Competition between elastase and related proteases from human neutrophil for binding to alpha1-protease inhibitor, *Am J Respir Cell Mol Biol.* **32**, 553-9.

41. Huntington, J. A., Read, R. J. & Carrell, R. W. (2000) Structure of a serpin-protease complex shows inhibition by deformation, *Nature.* **407**, 923-6.

42. Hajjar, E., Korkmaz, B., Gauthier, F., Brandsdal, B. O., Witko-Sarsat, V. & Reuter, N. (2006) Inspection of the binding sites of proteinase3 for the design of a highly specific substrate, *J Med Chem.* **49**, 1248-60.

43. Hajjar, E., Korkmaz, B. & Reuter, N. (2007) Differences in the substrate binding sites of murine and human proteinase 3 and neutrophil elastase, *FEBS Lett.* **581**, 5685-90.

44. Fu, Z., Thorpe, M., Akula, S., Chahal, G. & Hellman, L. T. (2018) Extended Cleavage Specificity of Human Neutrophil Elastase, Human Proteinase 3, and Their Distant Ortholog Clawed Frog PR3-Three Elastases With Similar Primary but Different Extended Specificities and Stability, *Front Immunol.* **9**, 2387.

45. Wiesner, O., Litwiller, R. D., Hummel, A. M., Viss, M. A., McDonald, C. J., Jenne, D. E., Fass, D. N. & Specks, U. (2005) Differences between human proteinase 3 and neutrophil elastase and their murine homologues are relevant for murine model experiments, *FEBS Lett.* **579**, 5305-12.

46. Rao, N. V., Wehner, N. G., Marshall, B. C., Gray, W. R., Gray, B. H. & Hoidal, J. R. (1991) Characterization of proteinase-3 (PR-3), a neutrophil serine proteinase. Structural and functional properties, *J Biol Chem.* **266**, 9540-8.

47. Korkmaz, B., Attucci, S., Hazouard, E., Ferrandiere, M., Jourdan, M. L., Brillard-Bourdet, M., Juliano, L. & Gauthier, F. (2002) Discriminating between the activities of human neutrophil elastase and proteinase 3 using serpin-derived fluorogenic substrates, *J Biol Chem.* **277**, 39074-81.

48. Cadene, M. & Chait, B. T. (2000) A robust, detergent-friendly method for mass spectrometric analysis of integral membrane proteins, *Anal Chem.* **72**, 5655-8.

49. Gabant, G. & Cadene, M. (2008) Mass spectrometry of full-length integral membrane proteins to define functionally relevant structural features, *Methods.* **46**, 54-61.

50. Burkert, U. & Norman, L. (1982) Allinger, Molecular Mechanics (ACS Monograph 177). Washington, DC, *American Chemical Society*.

51. ten Brink, T. & Exner, T. E. (2010) pK(a) based protonation states and microspecies for protein-ligand docking, *J Comput Aided Mol Des.* **24**, 935-42.

52. Korb, O., Stutzle, T. & Exner, T. E. (2009) Empirical scoring functions for advanced protein-ligand docking with PLANTS, *J Chem Inf Model.* **49**, 84-96.

53. Korb, O., Stützle, T. & Exner, T. E. (2006) PLANTS: Application of Ant Colony Optimization to Structure-Based Drug Design, *Lecture Notes in Comput Sci.* **4150**, 247-258

54. Korb, O., Stützle, T. & Exner, T. E. (2007) An ant colony optimization approach to flexible protein-ligand docking, *Swarm Intell.* **1**, 115-134.

55. Narawane, S., Budnjo, A., Grauffel, C., Haug, B. E. & Reuter, N. (2014) In silico design, synthesis, and assays of specific substrates for proteinase 3: influence of fluorogenic and charged groups, *J Med Chem.* **57**, 1111-5.

SUPPORTING INFORMATION

Supp.Table 1: LC-ESI-TQ MS and MALDI-TOF MS identification of oxidized insulin B-chain products of hPR3 proteolysis. The cleavage products were obtained by incubation for 95 min at 23 °C.

Supp.Figure 1: SDS-PAGE analysis of plasma α2-M processing by hPR3, hNE or hCatG.

Supp.Figure 2: Time-dependent generation of cleavages peptides upon proteolysis of insulin B-chain (570 µM) by hPR3 (0.835 µM).

Supp.Figure 3: Mass determination of the peptides generated after 95 min proteolysis of insulin B-chain by hPR3.

Supp.Figure 4: Identification of the cleavage sites within whole α2-M (16 µM) after incubation with hPR3 (0.5 µM).

Supp.Figure 5: Mass determination of the peptides generated after 3h proteolysis of 39pep-α2-M by hPR3 or hNE.

Table 1. Influence of P2 residues on the specificity constants k_{cat}/K_m for the hydrolysis of fluorogenic substrates by hPR3 and kNE. *Values are the means of n ≥ 4 experiments. The error for k_{cat}/K_m is < 15%. The P2 residues are shown in bold.*

		PROTEINASES	
		hPR3	*hNE*
SUBSTRATES		*k_{cat}/K_m ($mM^{-1}s^{-1}$)*	
1	ABZ-V A **D** (nor)V A D Y Q-EDDnp	7000*	n.s.h.
2	ABZ-V A **H** (nor)V A D Y Q-EDDnp	76	< 1
3	ABZ-V A **L** (nor)V A D Y Q-EDDnp	503	81
4	ABZ-V A **Y** (nor)V A D Y Q-EDDnp	3500	n.s.h.
5	ABZ-V A **P** (nor)V A D Y Q-EDDnp	2300	15
6	ABZ-V A **T** (nor)V A D Y Q-EDDnp	700	7
7	ABZ-V A **W** (nor)V A D Y Q-EDDnp	600	< 1
8	ABZ-V A **R** (nor)V A D Y Q-EDDnp	132	6.5
9	Biotin-P Y **D** (nor)V-AMC	468	n.s.h.
10	Biotin-P Y **H** (nor)V-AMC	36	n.s.h.
11	Biotin-P Y **L** (nor)V-AMC	34	22

n.s.h., no significant hydrolysis
* Value from [18]

Table 2. Specificity constants k_{cat}/K_m for the hydrolysis of fluorogenic substrates derived from the bait region of α2-M by hPR3 and hNE. *Values are the means of n ≥ 4 experiments. The error for k_{cat}/K_m is < 15%. The P2 residues are shown in bold. The P2 residues are shown in bold.*

		PROTEINASES	
		hPR3	*hNE*
SUBSTRATES		*k_{cat}/K_m ($mM^{-1}s^{-1}$)*	
12	ABZ-G R G H A R **L** V H V E E P H T-Y_{NO2}	35	1575
13	ABZ-G F Y E S **D** V M G R G-Y_{NO2}	<2	n.s.h.

n.s.h., no significant hydrolysis

.

FIGURE LEGENDS

Figure 1: Predicted cleavage site of hPR3 in the bait region of human α2-M according its proteolytic specificity. (A) SDS-PAGE analysis of hPR3-generated fragments of α2-M. 1 x 10^{-6} M of α2-M was incubated by hPR3 (0.1 and 0.5 x 10^{-6} M). At different times, the incubation mixtures were separated on a 10% SDS-PAGE gel denaturated/reduced conditions and visualized by silver nitrate staining. Similar results were obtained in three independent experiments. **(B)** The solvent-accessible surface of hPR3 active site was generated with Yasara (http://www.yasara.org) and colored to show positive (blue) and negative (red) electrostatic potentials. The serine of the catalytic triad is in yellow. The single letter code of critical charged residues in the vicinity of the active site is indicated in white. **(C)** Subsites preferences of PR3 obtained by kinetic analysis of the cleavage of synthetic substrates [3, 13, 14, 36, 55]. **(D)** P1 residues of potential hPR3 cleavage sites are shown by asterix. P2 residues (arginine, aspartate and histidine) which could alter hPR3 processing are colored. Arrows indicate identified cleavage sites of porcine pancreatic elastase (pPE), hCatG and hNE in α2-M bait region sequence [33].

Figure 2: Time-dependent generation of cleavage peptides upon cleavage of melittin and oxidized insulin B chain by hPR3 and hNE. The proteinase at a final concentration of 835 x 10^{-9} M was reacted with melittin (715 x 10^{-6} M) or oxidized insulin B chain (570 x 10^{-6} M) at pH 7.4 and 23 °C. Intact peptides and cleavage products were monitored by LC-MS and MALDI-TOF MS at 0, 7, 15, 45, 95, 240, 420 and 1320 min. Arrows were drawn according to the chronological order of appearance of the cleavage peptides deduced from the kinetic profiles. Large arrows indicate major (early cleaved) sites. Thin or dashed arrows indicate minor (late cleaved) sites. The hydrophilic or negatively charged residues at P2 of the hPR3 cleavage site are framed. The cysteic acids are circled.

Figure 3: Identification of the cleavage sites within ABZ-VAL(nor)VADYQ-EDDnp after hydrolysis by hPR3 and hNE. (A) Reversed-phase HPLC chromatograms of the substrate after hydrolysis by hPR3 and hNE. Absorbances at 220 nm (peptidyl bond, blue) and 360 nm (EDDnp, green) are reported. 20 x 10^{-6} M of ABZ-VAL(nor)VADYQ-EDDnp are incubated with 5 x 10^{-8} M of hPR3 or hNE during 2 h at 37 °C. **(B)** Arrows indicate the cleavage sites that were identified by N-terminal sequencing of the EDDnp-containing fragments having an absorbance peak at 360 nm.

Figure 4: Proposed putative models of AMC substrates binding to the active site of hPR3. The computational molecular docking showed that the P2 residue in fluorogenic substrates Biotin-PY**D**(nor)Val-AMC, Biotin-PY**H**(nor)Val-AMC and Biotin-PY**L**(nor)Val-AMC were close to solvent accessible positively charged Lys^{99} in hPR3 active site. The models were generated using the

molecular docking programme (PLANTS v. 1.2) and the visualization of the solvent-accessible surface of hPR3 in complexes with the substrate was obtained using programme PyMOL v. 1.3.

Figure 5: Identification of the cleavage sites within whole α2-M (16 µM) after incubation with hPR3 (0.5 µM) at pH 8.5 and 37 °C. Cleavage products were monitored by MALDI-TOF MS. The width of arrows reflects how early cleavages are observed (20 s or 60 min), and takes into account the relative intensity of peptide peaks that differ by a few amino acids. The bait region sequence is shown in blue.

Figure 6: Time dependent generation of cleavage products upon cleavage of α2-M bait region sequence-derived peptide by hPR3 and hNE. (**A**) The 39-residue bait region peptide (39pep-α2M) (50 x 10^{-6} M) was incubated with 5 x 10^{-8} M of hPR3 or 1 x 10^{-9} M hNE for 3 h at 37 °C and the peptides produced upon proteolysis were separated by RP-HPLC on a C18 column. (**B**) MALDI-TOF MS was used to measure the mass of the peptides purified by RP-HPLC as shown in A. Arrows indicate the cleavage sites of hPR3 and hNE that were identified. The width of arrows indicates the intensity of the cleavage.

ACKNOWLEDGMENTS

This work was supported by “Région Centre-Val de Loire" (PIRANA, SyMBioMS, MALDITOF) and the European FEDER program (2017-EX002979). The authors thank C. Epinette (INSERM U-1100) for excellent technical assistance and Dr. P. Davies and Dr J.L. Humes from Merck for the kind gift of hPR3.

AUTHOR CONTRIBUTIONS

B. Korkmaz, K. N’Guessan, A. van Dorsselaer, J.G. Bieth and M. Cadene planed experiments; K. N’Guessan, R. Grzywa, S. Seren, G. Gabant, C. Kellenberger, M. Cadene, M. Moniatte, M. Juliano performed experiments; B. Korkmaz, M. Cadene, F. Gauthier, A. Lesner, M. Sieńczyk, M. Moniatte analyzed the data; B. Korkmaz wrote the manuscript. Authors contributed to the writing and revision process of the manuscript. B. Korkmaz supervised the work.

CONFLICTS OF INTEREST

The authors declare that they have no conflicts of interest

A

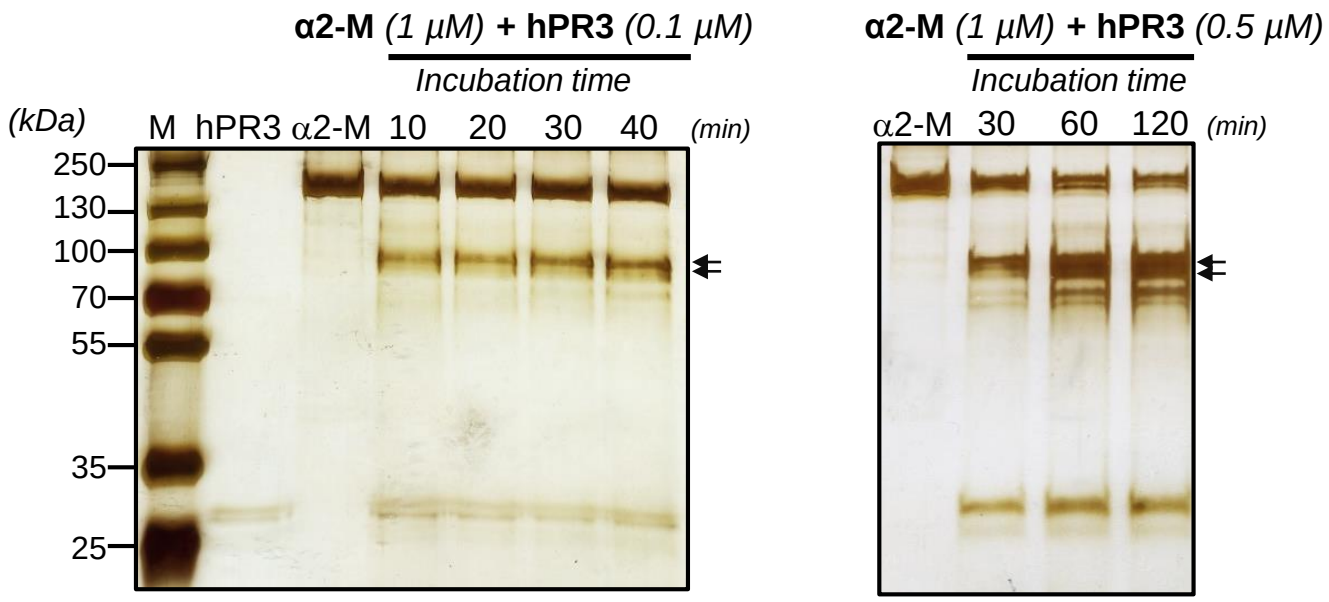

B

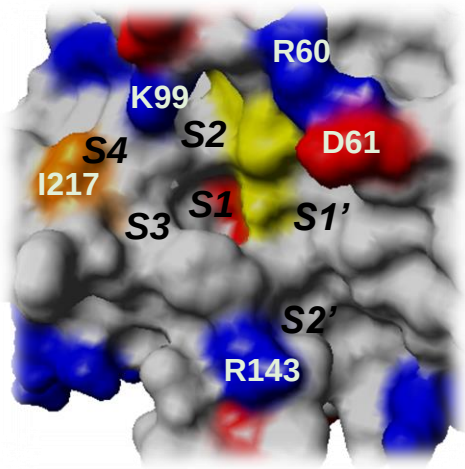

C

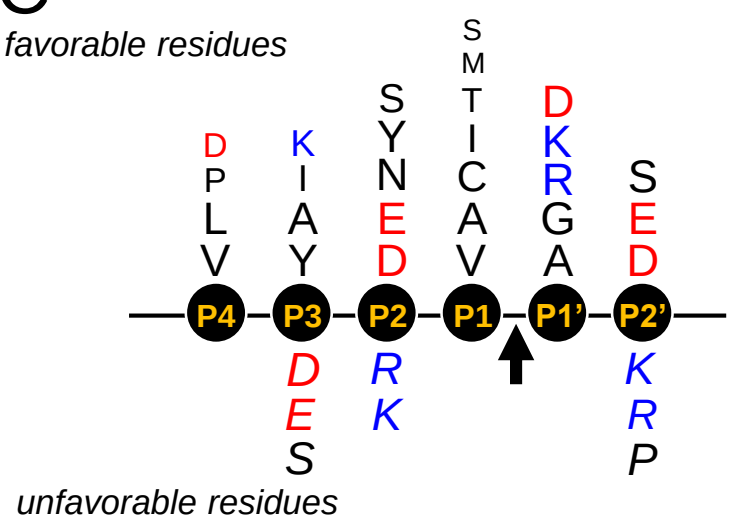

D

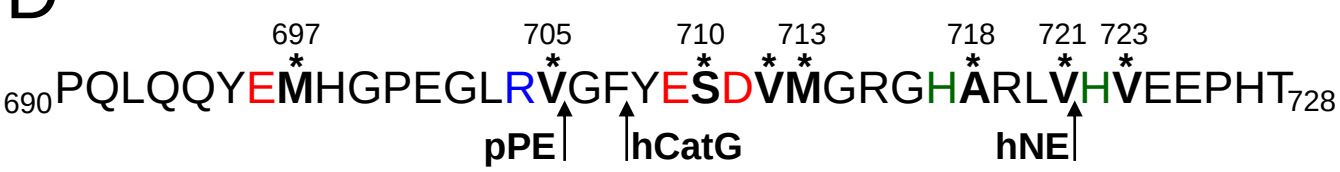

α2-M bait region sequence

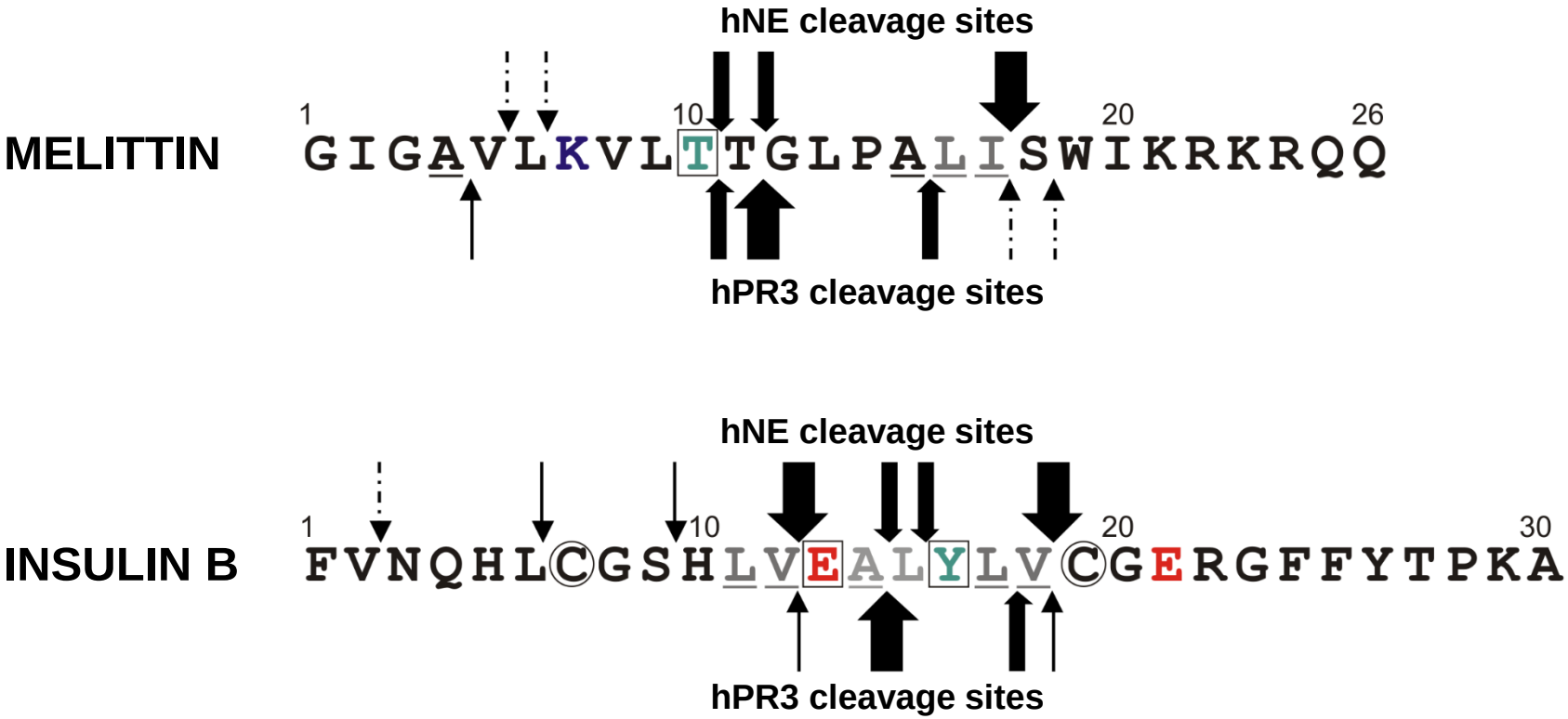
hNE cleavage sites
MELITTIN
1
10
20
26
GIGAVLKVLTTGLPALISWIKRKRQQ
hPR3 cleavage sites
hNE cleavage sites
INSULIN B
1
10
20
30
FVNQHLCGSHLVEALYLVCGERGFFYTPKA
hPR3 cleavage sites

A

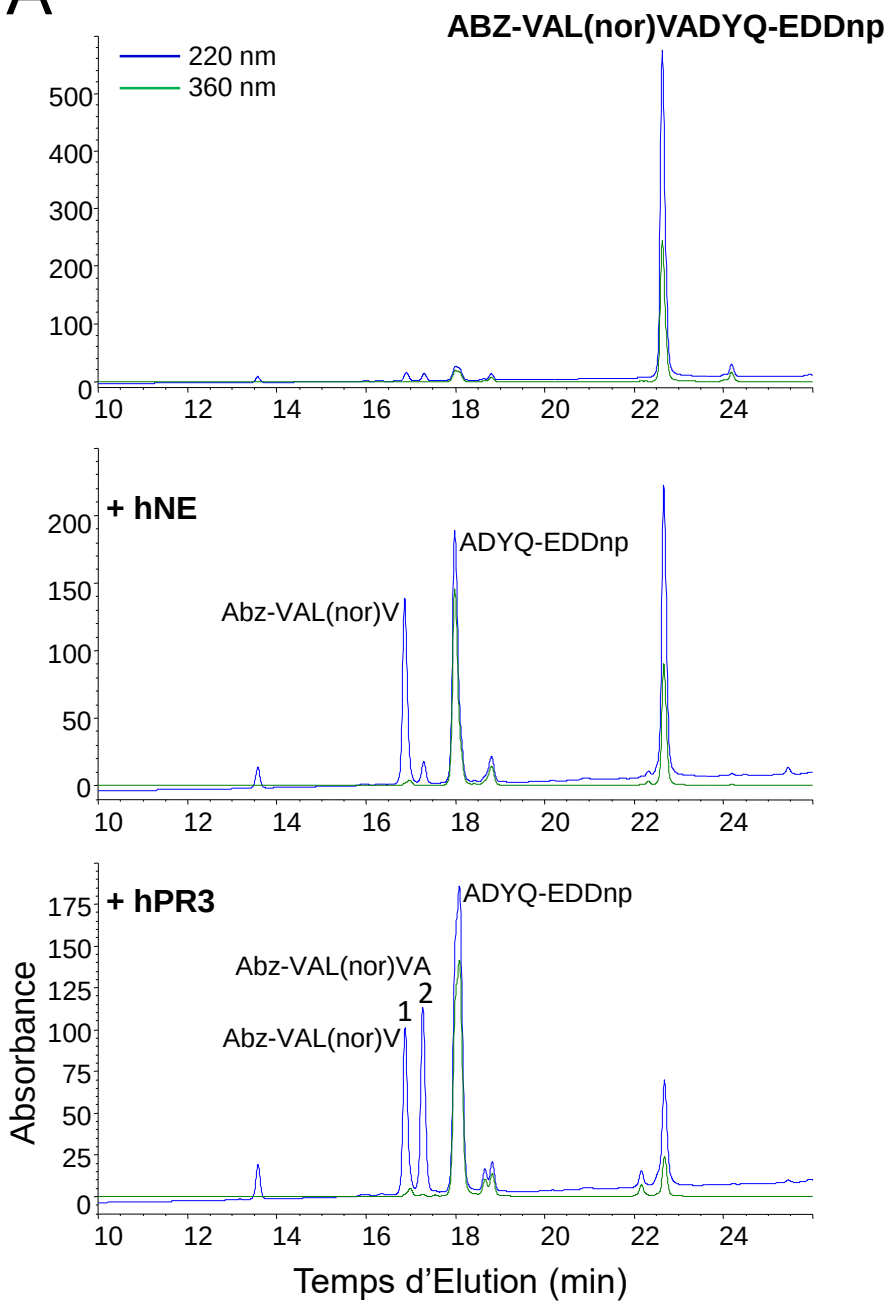
ABZ-VAL(nor)VADYQ-EDDnp
220 nm
360 nm
+ hNE
ADYQ-EDDnp
Abz-VAL(nor)V
+ hPR3
ADYQ-EDDnp
Abz-VAL(nor)VA
1
2
Abz-VAL(nor)V
Absorbance
Temps d'Elution (min)

B

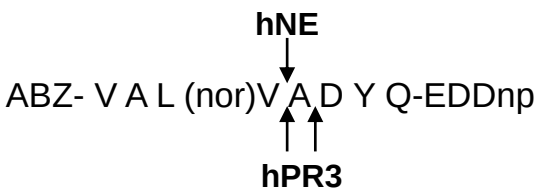
hNE
ABZ- V A L (nor)V A D Y Q-EDDnp
hPR3

A

Biotin-PY**D**(nor)V-AMC

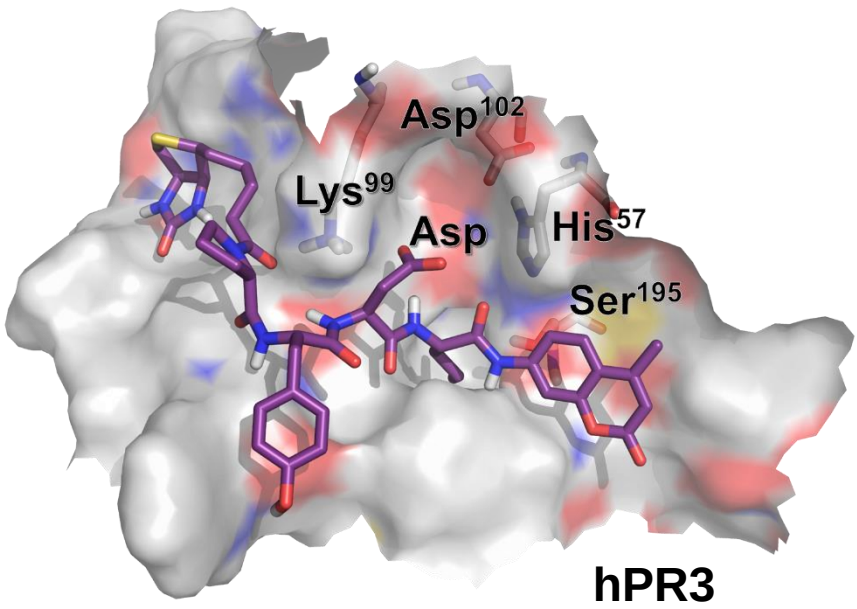

B

Biotin-PY**H**(nor)V-AMC

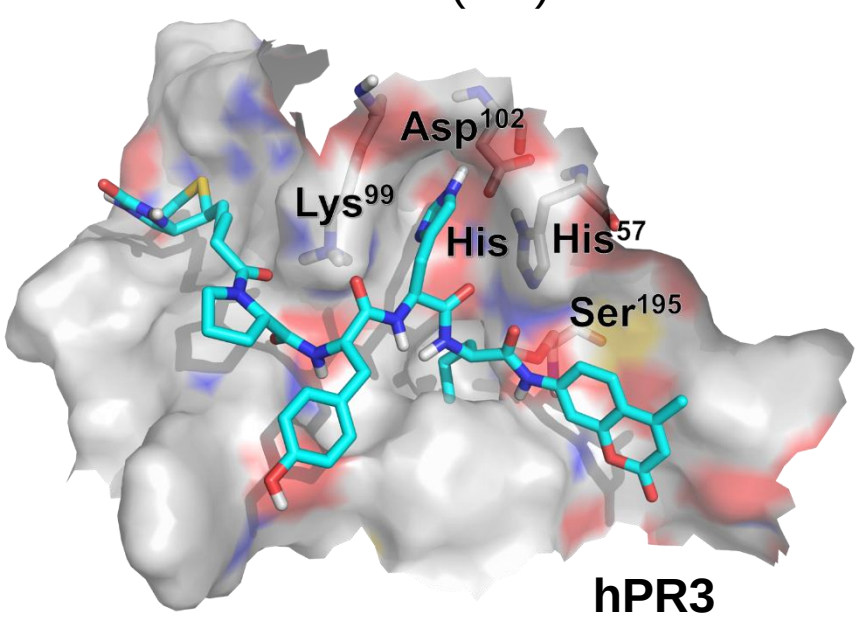

C

Biotin-PY**L**(nor)V-AMC

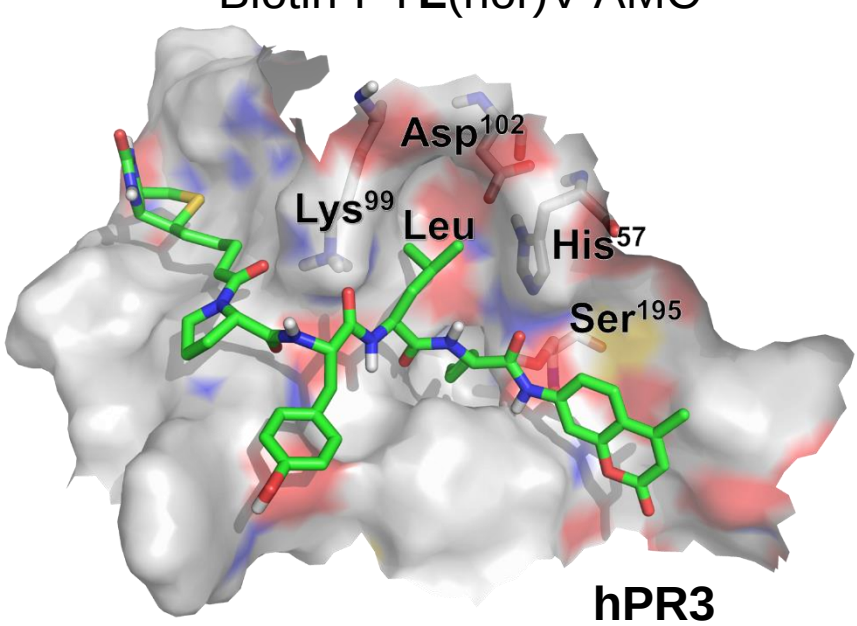

- **t = 20 s**

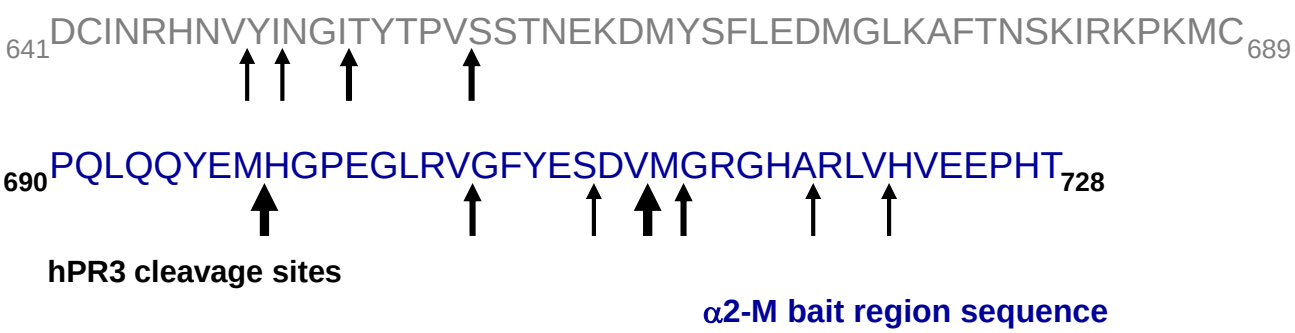
641DCINRHNVYINGITYTPVSSTNEKDMYSFLEDMGLKAFTNSKIRKPKMC689
690PQLQQYEMHGPEGLRVGFYESDVMGRGHARLVHVEEPHT728
hPR3 cleavage sites
α2-M bait region sequence

- **t = 60 min**

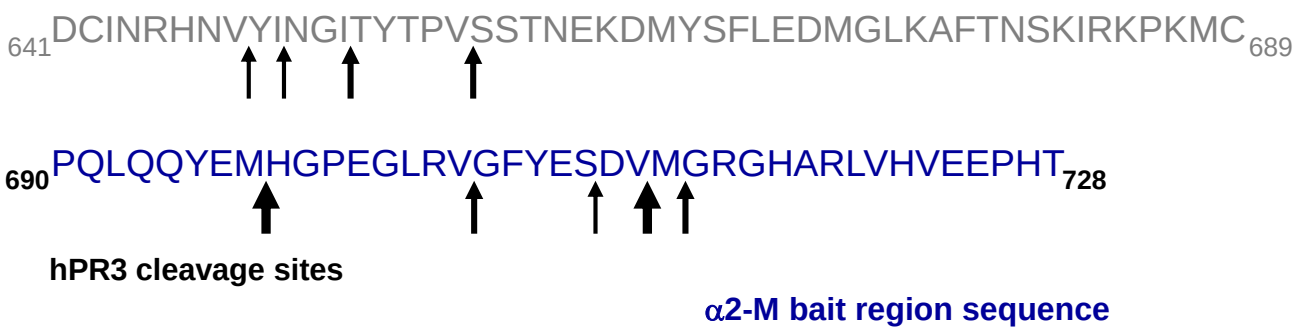
641DCINRHNVYINGITYTPVSSTNEKDMYSFLEDMGLKAFTNSKIRKPKMC689
690PQLQQYEMHGPEGLRVGFYESDVMGRGHARLVHVEEPHT728
hPR3 cleavage sites
α2-M bait region sequence

A

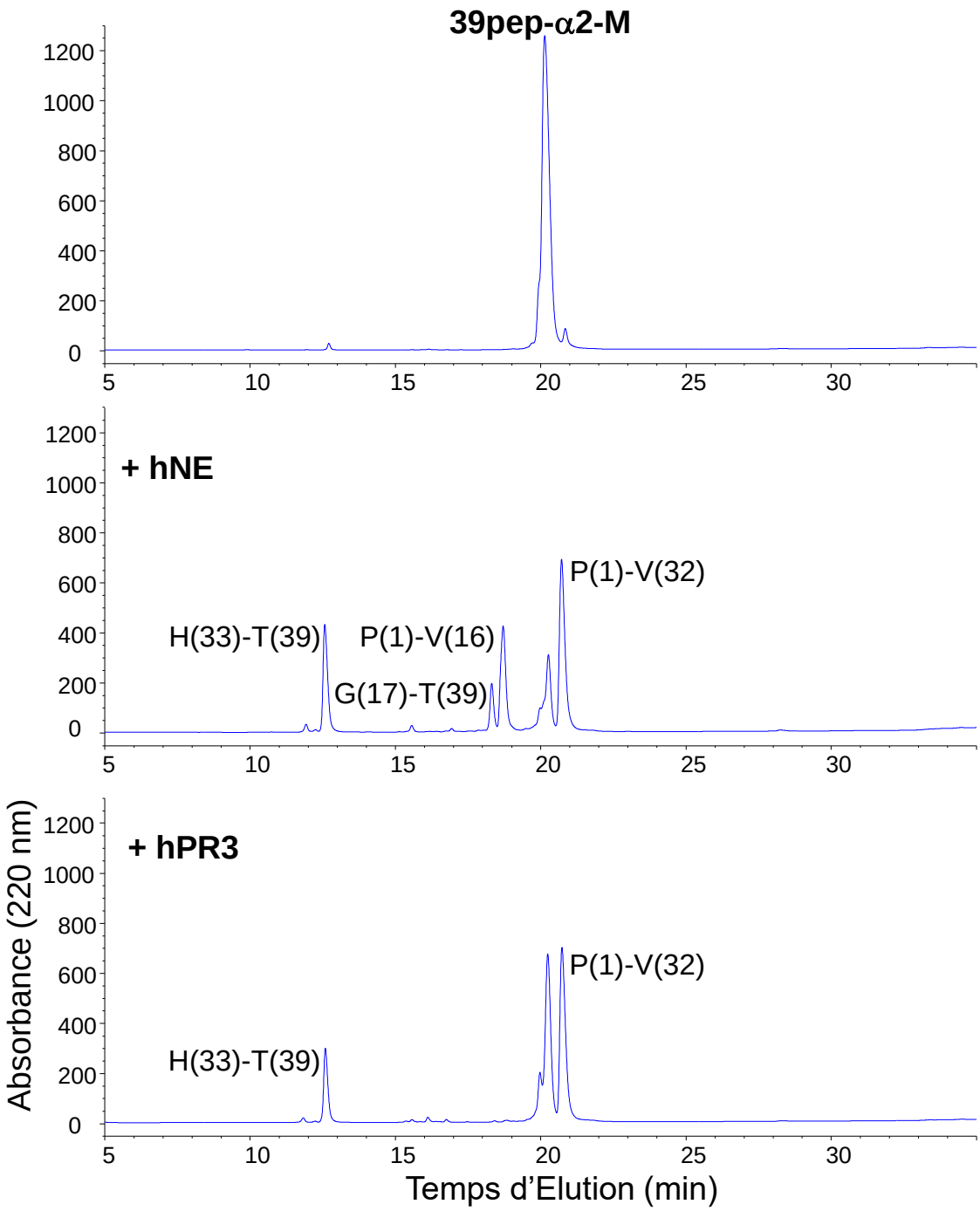
39pep-α2-M
+ hNE
H(33)-T(39)
P(1)-V(16)
G(17)-T(39)
P(1)-V(32)
+ hPR3
H(33)-T(39)
P(1)-V(32)
Absorbance (220 nm)
Temps d'Elution (min)

B

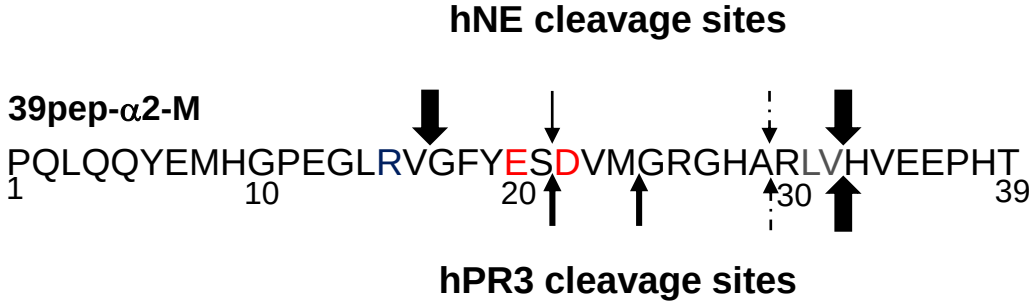
hNE cleavage sites
39pep-α2-M
PQLQQYEMHGPEGLRVGFYESDVMGRGHARLVHVEEPHT
1
10
20
30
39
hPR3 cleavage sites

hPR3

-VMGRGHARLV HVEEPHT- *39pep-α2-M*

UNFAVORABLE P2 RESIDUES